

A non-linear solution to the S_8 tension?

Alexandra Amon^{1*}, George Efstathiou^{1†}

¹ *Kavli Institute for Cosmology Cambridge, Madingley Road, Cambridge, CB3 0HA.*

24 June 2022

ABSTRACT

Weak galaxy lensing surveys have consistently reported a lower amplitude for the matter fluctuation spectrum, as measured by the S_8 parameter, than expected in the Λ CDM cosmology favoured by *Planck*. However, the expansion history follows the predictions of the *Planck* Λ CDM cosmology to high accuracy, as do measurements of lensing of the cosmic microwave background anisotropies. Redshift space distortion measurements also appear to be consistent with *Planck* Λ CDM. In this paper, we argue that these observations can be reconciled with the *Planck* Λ CDM cosmology if the matter power spectrum is suppressed more strongly on non-linear scales than assumed in analyses of weak galaxy lensing. We demonstrate this point by fitting a one-parameter model, characterising a suppression of the non-linear power spectrum, to the KiDS-1000 weak lensing measurements. Such a suppression could be attributed to new properties of the dark matter that affect non-linear scales, or to a response of the matter fluctuations to baryonic feedback processes that are stronger than expected from recent cosmological simulations. Our proposed explanation can be tested using measurements of the amplitude of the matter fluctuation spectrum on linear scales, in particular via high precision redshift space distortion measurements from forthcoming galaxy and quasar redshift surveys.

Key words: cosmology: cosmological parameters, weak lensing, observations

1 INTRODUCTION

The standard Λ CDM cosmological model provides a remarkably good fit to a number of observations, including anisotropies of the cosmic microwave background (CMB; e.g. Bennett et al. 2013; Planck Collaboration et al. 2020a; Aiola et al. 2020; Dutcher et al. 2021), baryon acoustic oscillations (BAO; e.g. Alam et al. 2017; Blomqvist et al. 2019; de Sainte Agathe et al. 2019; Alam et al. 2021) and the magnitude-redshift relation of Type Ia supernovae (e.g. Betoule et al. 2014; Scolnic et al. 2017; Brout et al. 2021). Despite these successes, there is some evidence of ‘tensions’ with other astrophysical data at varying degrees of statistical significance.

At the level of the background expansion history, some late time measurements of the Hubble constant disagree with the Λ CDM value inferred from the CMB (e.g. Riess et al. 2016, 2019, 2021; Wong et al. 2020) though others do not (Freedman et al. 2019, 2020). This problem has become known as the ‘Hubble tension’ (for recent reviews see Freedman 2021; Shah et al. 2021; Abdalla et al. 2022).

At the level of perturbations, weak lensing surveys have reported measurements of the amplitude of the fluctuation spectrum (e.g. Heymans et al. 2013; Hikage et al. 2019;

Hamana et al. 2020; Asgari et al. 2021; Amon et al. 2022b; Secco et al. 2022). Specifically, cosmic shear surveys tightly constrain the parameter combination¹ $S_8 = \sigma_8(\Omega_m/0.3)^{0.5}$, consistently finding values that are lower than that expected according to the *Planck* best fit Λ CDM cosmology. This discrepancy has become known as the ‘ S_8 tension’. Most recently, two large cosmic shear surveys have reported new constraints. Assuming a spatially flat Λ CDM cosmology, the Kilo-Degree Survey (KiDS)-1000 gives²:

$$S_8 = \begin{cases} 0.759^{+0.024}_{-0.021}, & \text{KiDS-1000 cosmic shear,} \\ 0.766^{+0.020}_{-0.014}, & \text{KiDS-1000 } 3 \times 2\text{pt,} \end{cases} \quad (1)$$

see Asgari et al. (2021) for the shear-shear analysis (hereafter KiDS21) and Heymans et al. (2021) for a $3 \times 2\text{pt}$ analysis combining shear-shear, galaxy-galaxy lensing and galaxy-galaxy two-point statistics. The Dark Energy Survey (DES)

¹ Where Ω_m is the present day matter density in units of the critical density, σ_8 is the root mean square linear amplitude of the matter fluctuation spectrum in spheres of radius $8h^{-1}\text{Mpc}$ extrapolated to the present day, and h is the value of the Hubble constant H_0 in units of $100 \text{ km s}^{-1} \text{ Mpc}^{-1}$.

² We quote results derived from the COSEBI (complete orthogonal sets of E/B integrals, see Schneider et al. (2010)) statistics.

* E-mail: alexandra.amon@ast.cam.ac.uk

† E-mail: gpe@ast.cam.ac.uk

Year 3 analysis gives

$$S_8 = \begin{cases} 0.772^{+0.018}_{-0.017}, & \text{DES Y3 cosmic shear,} \\ 0.779^{+0.014}_{-0.015}, & \text{DES Y3 } 3 \times 2\text{pt} \end{cases} \quad (2)$$

where we have quoted the ‘ Λ CDM optimised’ results for the shear-shear analysis (Amon et al. 2022b; Secco et al. 2022), hereafter DES22, and for the 3x2pt function analysis (DES Collaboration et al. 2021). The results quoted above are derived using different analysis choices (angular scale cuts, intrinsic alignment model, etc.) and differences in assumptions concerning neutrino masses³.

For *Planck*, we adopt the Λ CDM parameters reported in Efstathiou & Gratton (2021) (hereafter EG21):

$$S_8 = 0.828 \pm 0.016, \quad \text{TTTEEE}, \quad (3a)$$

$$S_8 = 0.829 \pm 0.012, \quad \text{TTTEEE} + \text{Plens}, \quad (3b)$$

where TTTEEE denotes the high multipole likelihood constructed by combining the temperature power spectra (TT), temperature-polarization E-mode cross-spectra (TE) and polarization E-mode power spectra (EE). Each of these likelihoods is combined with low multipole ($\ell \leq 29$) TT and EE likelihoods described in Planck Collaboration et al. (2020a). ‘Plens’ in Eq. (3b) denotes the addition of the *Planck* CMB lensing likelihood (Planck Collaboration et al. 2020b).

The KiDS-1000 cosmic shear measurements of S_8 are about 9% lower than the *Planck* value of Eq. (3b), suggesting a discrepancy at the $\sim 2.4 - 2.7\sigma$ level⁴ depending on which of the KiDS-1000 and *Planck* measurements are used in the comparison. This is consistent with the conclusions of the KiDS team based on more complex tension metrics (Asgari et al. 2021; Heymans et al. 2021). The DES Y3 measurements are about 7% lower than the *Planck* value, suggesting a discrepancy at about the $\sim 2.3 - 2.6\sigma$ level⁵. To simplify the analysis in this paper, we focus on the cosmic shear measurement since it is the dominant contribution in the $3 \times 2\text{pt}$ S_8 constraint and therefore the driver of the S_8 tension.

While neither of the lensing surveys taken in isolation offers decisive evidence for a discrepancy with the *Planck* Λ CDM cosmology, both surveys find low values of S_8 in agreement with earlier work. It therefore seems unlikely that the S_8 tension is simply a statistical fluctuation. However, we note that it is naive to crudely combine the shear estimates in Eqs (1) and (2), as these analyses use different modelling frameworks, cosmological priors, angular ranges and various other analysis choices such as to the modelling of intrinsic alignments (IA)⁶.

³ The *Planck* and KiDS analyses assume a normal hierarchy with the heaviest neutrino mass fixed to 0.06 eV, while DES allows the neutrino mass to vary, which has little impact on their S_8 constraints (DES Collaboration et al. 2021, Fig. 28).

⁴ We quote $\Delta S_8 / \sqrt{(\sigma_{S_8}^{\text{Planck}})^2 + (\sigma_{S_8}^{\text{lensing}})^2}$.

⁵ The DES team exclude *Planck* lensing when comparing their results with *Planck*. As can be seen from Eqs (3a)-(3b) adding *Planck* lensing reduces the error on S_8 , increasing the significance of the discrepancy with the DES Y3 results.

⁶ A combined shear-shear analysis of DES Y3 and KiDS-1000, including a detailed analysis of the differences in methodology and analysis choices, is currently in preparation by the KiDS and DES collaborations.

In the last few years there have been significant advances in the calibration of the lensing data (see Asgari et al. 2020; Amon et al. 2022b, and references therein). Improved methods of calibrating photometric redshifts (Hildebrandt et al. 2021; Myles et al. 2021) show that errors in the redshift distributions of the source galaxies are unlikely to account for a $\sim 7\% - 9\%$ discrepancy in value of S_8 . It also seems implausible that systematic errors in the shear measurements could explain a discrepancy of this size (Mandelbaum et al. 2018; Kannawadi et al. 2019; MacCrann et al. 2022). Similarly, the modelling of IA may affect the value of S_8 at the one or two percent level (given the small amplitudes of the alignment corrections found by KiDS and DES) but it seems unlikely that IA are responsible for a $\sim 7\%$ discrepancy.

What is the most likely explanation of this S_8 tension? Does it require a radical departure from the Λ CDM paradigm? We explore both of these questions in this paper. This paper is structured as follows. Section 2 discuss some preliminaries including comparisons with other types of data which serve as pointers towards an explanation. The main results of this paper are contained in Section 3, which explores the sensitivity of weak lensing results to the modelling of the matter power spectrum on non-linear scales. We discuss the implications of our findings in Section 4 and summarize our conclusions in Section 5.

2 PRELIMINARIES

2.1 The S_8 tension

In this paper, we focus exclusively on the KiDS-1000 shear-shear results, adopting their fiducial analysis pipeline and modelling choices⁷. Fig. 1 shows the KiDS21 constraints in the $S_8 - \Omega_m$ plane from the publicly released MCMC chains⁸. Asgari et al. (2021) present results for three two-point statistics: the usual shear two-point correlation functions ξ_{\pm} , COSEBIs (which KiDS21 adopt as their default for parameter analysis) and angular power spectra. The COSEBIs and power spectra are estimated by integrating over the correlation functions, thus any model that fits ξ_{\pm} over the full angular range probed by KiDS should be consistent with the COSEBIs and power spectra. Fig. 1 also shows constraints from *Planck*. The red contours show the constraints from the DES Y3 shear-shear analysis (Amon et al. 2022a; Secco et al. 2022). As noted above, S_8 from DES Y3 is slightly higher but statistically consistent with the values determined from the KiDS analysis.

The S_8 tension between *Planck* and cosmic shear summarized in Sect. 1 is clearly evident and is particularly acute if one compares *Planck* TTTEEE+Plens to the KiDS ξ_{\pm} results. One can also see that the KiDS ξ_{\pm} contours, whilst overlapping with the COSEBI contours, are shifted to lower values of Ω_m . The ξ_{\pm} and the COSEBI analyses differ primarily in the range of spatial scales sampled by the statistics, with the ξ_{\pm} contours more sensitive to small scales (Asgari et al. 2021). We will focus on the KiDS ξ_{\pm} measurements in

⁷ KiDS Cosmology Analysis Pipeline: <https://github.com/KiDS-WL/kcap>

⁸ <http://kids.strw.leidenuniv.nl/sciencedata.php>

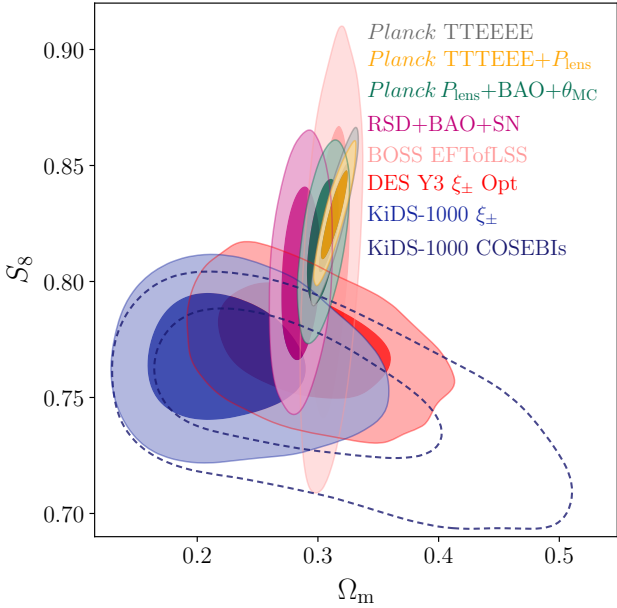


Figure 1. 68% and 95% constraints in the $S_8 - \Omega_m$ plane for various data. The blue and navy (dashed) show the constraints from the KiDS ξ_{\pm} and COSEBI statistics as analyzed by KiDS21, while the red shows that from the DES Y3 Λ CDM optimised ξ_{\pm} analysis. The yellow and grey contours show constraints from *Planck* TTTEEE with and without the addition of the *Planck* CMB lensing likelihood (Plens). The peach contours labelled EFTofLSS represent constraints from the BOSS power spectrum and bispectrum effective field theory analysis of D’Amico et al. (2022). The magenta contours show constraints from redshift space distortions (RSD) combined with BAO and SN measurements as described in the text. The green contours show the constraint from the *Planck* lensing likelihood combined with BAO together with conservative priors on the acoustic peak location parameter θ_{MC} and other cosmological parameters (Planck Collaboration et al. 2020b).

this paper, though we discuss the COSEBI measurements in Appendix A.

2.2 Constraints from redshift space distortions

Redshift space distortions (RSD) provide an independent way to measure the growth rate of fluctuations (Kaiser 1987). RSD provide a measurement of the parameter combination $f\sigma_8$, where f is the logarithmic derivative of the linear growth rate D with respect to the scale factor

$$f = \frac{d \ln D}{d \ln a}, \quad (4)$$

and $a = (1+z)^{-1}$. In the Λ CDM model, $f \approx \Omega_m(z)^{0.55}$ (Lahav et al. 1991). RSD measurements from large galaxy redshift surveys are of particular relevance to the S_8 tension because they overlap with the redshift range covered by the KiDS survey. Since most of the information on RSD from the analyses discussed in this section comes from wavenumbers in the range $0.01 h\text{Mpc}^{-1} \lesssim k \lesssim 0.1 h\text{Mpc}^{-1}$ (see, for example, Fig. 8 of Philcox & Ivanov 2021) corresponding to linear or very mildly non-linear scales, any discrepancy with the

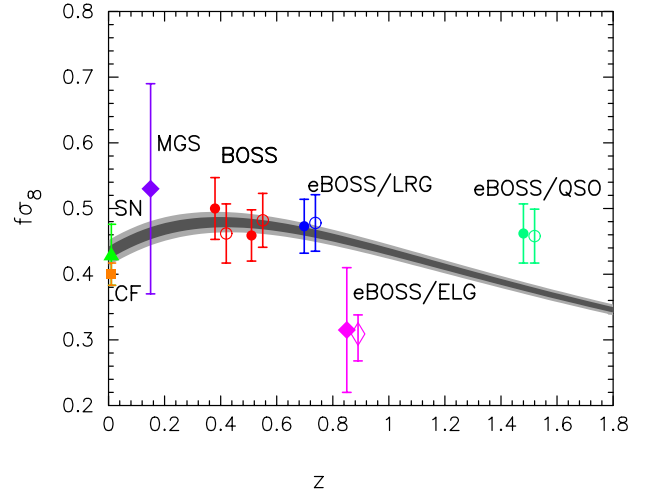


Figure 2. Measurements of $f\sigma_8$ from various surveys. The green triangle at $z_{\text{eff}} = 0.02$ is from an analysis of low redshift Type Ia SN by Huterer et al. (2017) and the orange square is from the cosmic flows analysis of Boruah et al. (2020) using SN, surface brightness fluctuations and Tully-Fisher distances to nearby galaxies. The filled symbols are from the consensus results from the completed BOSS/eBOSS surveys (Alam et al. 2021). The measurement at $z = 0.15$ is for the SDSS Main Galaxy Sample (Howlett et al. 2015). The open circles show a reanalysis of the BOSS, eBOSS/LRG and eBOSS/QSO samples by Brieden et al. (2022) using their *ShapeFit* methodology. The open diamond shows results from an effective field theory analysis of the eBOSS Emission Line Galaxy sample by Ivanov (2021). The grey bands show the 1σ and 2σ regions allowed by the *Planck* base Λ CDM cosmology.

Planck Λ CDM model would be fatal to the explanation of the S_8 tension proposed in this paper. It is therefore important to review the consistency between RSD measurements and the *Planck* Λ CDM model in detail.

As noted in Planck Collaboration et al. (2016), early RSD measurements used a fixed fiducial cosmology that differed significantly from the *Planck* Λ CDM cosmology leading to potential biases and underestimates of the error on $f\sigma_8$ (Howlett et al. 2015). In addition, there have been significant theoretical advances in the modelling of RSD in recent years. To compute the RSD constraints in Fig. 1 we have used the results shown by the filled symbols in Fig. 2. The measurements at $z_{\text{eff}} = 0.38$ and 0.61 are the ‘consensus’ results from the completed Baryon Oscillation Spectroscopy Survey (BOSS) and extended BOSS (eBOSS) surveys (Alam et al. 2017, 2021)⁹ supplemented by the the measurement from the SDSS Main Galaxy Sample (MGS) at $z_{\text{eff}} = 0.15$ (Ross et al. 2015; Howlett et al. 2015) and the low redshift ($z_{\text{eff}} \approx 0.02$) measurements of $f\sigma_8$ from Huterer et al. (2017) and Boruah et al. (2020) from peculiar velocity-density field correlations (which we loosely bracket under the term ‘RSD’ in this section). The grey contours in Fig. 2 show the 1σ and 2σ ranges contours for the *Planck* base Λ CDM cosmology.

The pink contours in Fig. 1 show the constraints in the

⁹ SDSS: <https://www.sdss.org/science/final-bao-and-rsd/-measurements-table>

S_8 - Ω_m plane derived by combining these RSD measurements (including the BAO constraints for the BOSS, eBOSS and MGS samples) with the Pantheon supernova magnitude-redshift relation (Scolnic et al. 2017), Ly α -quasar and Ly α -Ly α BAO measurements from (Blomqvist et al. 2019; de Sainte Agathe et al. 2019) and BAO measurements from the 6dF Galaxy Survey Beutler et al. (2011). To scale the BAO constraints we impose a Gaussian *Planck* prior on the sound horizon, $r_d = 147.31 \pm 0.31$ Mpc. The RSD constraints in Fig. 1 are consistent with the S_8 results from *Planck* TT-TEEE. There is also substantial overlap between the RSD and KiDS contours in Fig. 1.

The consensus RSD measurements plotted in Fig. 2 assume a *Planck* Λ CDM fiducial power spectrum with adjustable BAO location parameters in addition to the velocity fluctuation amplitude $f\sigma_8$. Recently, several groups have developed ‘full-shape’ analyses based on effective field theory (EFT) descriptions of non-linear perturbations (e.g. d’Amico et al. 2020; Ivanov et al. 2020; Chen et al. 2022b; Philcox & Ivanov 2021; D’Amico et al. 2022). The EFT analyses aim to constrain cosmological parameters independently of *Planck*. However, the nuisance parameters required to model perturbation theory counter-terms, galaxy biasing, and redshift space distortions, effectively down-weight information at wavenumbers $k \gtrsim 0.2h^{-1}\text{Mpc}$. As a consequence of the restricted wavenumber range, the primordial spectral index n_s is poorly constrained in comparison to *Planck*. Constraining n_s to the *Planck* best fit value, Ivanov et al. (2020) find $\sigma_8 = 0.721 \pm 0.43$, Philcox & Ivanov (2021) find $\sigma_8 = 0.729 \pm 0.040$ and Chen et al. (2022b) find $\sigma_8 = 0.738 \pm 0.048$, from fits to the BOSS power spectra. These are consistent with each other, but sit low compared to the *Planck* Λ CDM estimate, $\sigma_8 = 0.8095 \pm 0.0074$, by $1.6 - 2\sigma$ (see also Tröster et al. (2020)). The recent EFT analysis of the BOSS power spectrum and bispectrum (D’Amico et al. 2022) finds $\sigma_8 = 0.794 \pm 0.037$ (labelled as $P_\ell + B_0^{\text{loop}} + B_2^{\text{tree}}$ in their analysis) in good agreement with both the *Planck* Λ CDM value, as well as the cosmic shear results¹⁰. Constraints in the $S_8 - \Omega_m$ plane from this analysis are shown by the peach contours in Fig. 1.

Recently, Brieden et al. (2021b,a) have developed an extension of the ‘classical’ BOSS/eBOSS analyses, by including an additional parameter that is sensitive to the parameter combination $\Omega_m h$. The constraints on $f\sigma_8$ derived by applying their *ShapeFit* technique to the BOSS, eBOSS/LRG and eBOSS/QSO samples (Brieden et al. 2022) are shown by the open symbols in Fig. 2. These agree almost perfectly with the consensus results from the BOSS/eBOSS collaborations reported in Alam et al. (2017, 2021).

The open diamond in Fig. 2 shows the constraint $f\sigma_8(z_{\text{eff}} = 0.85) = 0.309^{+0.029}_{-0.041}$ from a full shape EFT analysis of the eBOSS/ELG sample by Ivanov (2021). This estimate is in strong disagreement with the *Planck* base Λ CDM value (by $\sim 4.7\sigma$) and also disagrees with the Λ CDM parameters determined from the BOSS DR12 sample (see their Fig. 1). The Ivanov (2021) eBOSS/ELG estimate of $f\sigma_8$ is clearly an outlier in Fig. 2, suggesting that further work is

¹⁰ Note that D’Amico et al. (2022) apply a correction for prior volume effects in the EFT analysis that bias σ_8 low by about 1σ if left uncorrected.

required to establish whether the shape of the power spectra is robust to the large corrections required to account for selection biases in the eBOSS/ELG sample.

Evidently, there are still small methodological differences in the RSD analyses that lead to differences of $\sim 1-2\sigma$ in measurements of $f\sigma_8$ inferred from the same data. Although the pink contours in Fig. 1 are consistent with the constraints from *Planck*, they have substantial overlap with the KiDS and DES contours. RSD measurements cannot yet distinguish decisively between the *Planck* and weak lensing amplitudes (Efstathiou & Lemos 2018; Nunes & Vagnozzi 2021). There is therefore no compelling evidence from RSD to support claims that linear growth rates are suppressed at redshifts $z \lesssim 1$ compared to the expectations of Λ CDM (Macaulay et al. 2013; Nesseris et al. 2017; Kazantzidis & Perivolaropoulos 2018; Benisty 2021; Abdalla et al. 2022).

Note also that the functional form of the linear growth rate $D(t)$ over the redshift range $\sim 0.2 - 0.7$ inferred from a tomographic analysis of cosmic shear, galaxy clustering and CMB lensing appears to be compatible with that expected in the Λ CDM model (García-García et al. 2021), though the overall fluctuation amplitude is found to be lower than expected in the *Planck* base Λ CDM cosmology.

2.3 CMB lensing

Rather than reflecting anomalies in the growth rate of perturbations, the S_8 tension may be related to anomalies in the propagation of photons, for example a departure from General Relativity that results in a ‘gravitational slip’ (e.g. Daniel et al. 2008; Bertschinger 2011; Simpson et al. 2013; Pizzuti et al. 2019). This can be tested using CMB gravitational lensing. The CMB lensing signal is caused by matter distributed along the line-of-sight over a broad redshift range with a median redshift of $z \sim 2$. This is not very much higher than the mean redshift $z \sim 1$ of the highest tomographic redshift bin in KiDS-1000 (which contributes the highest weight to the KiDS two point statistics).

As noted in Planck Collaboration et al. (2020b) for base Λ CDM with ‘lenspriors’ imposed¹¹, the *Planck* lensing likelihood tightly constrains the parameter combination¹²

$$\sigma_8 \Omega_m^{0.25} = 0.589 \pm 0.020, \quad \text{Plens}, \quad (5a)$$

which is within 1σ of the constraint derived from the TT-TEEE likelihood,

$$\sigma_8 \Omega_m^{0.25} = 0.6057 \pm 0.0081. \quad \text{TTEEE}. \quad (5b)$$

The addition of BAO data and a conservative prior of $\theta_{\text{MC}} = 1.0409 \pm 0.0006$ ¹³ (effectively adding another

¹¹ These are loose priors of $n_s = 0.96 \pm 0.02$, $\Omega_b h^2 = 0.0222 \pm 0.005$ (motivated by the deuterium abundance (Cooke et al. 2018)), $0.4 < h < 1$, and the optical depth to reionization fixed at $\tau = 0.055$.

¹² As this paper was nearing completion Carron et al. (2022) presented results from an improved *Planck* lensing likelihood. This gives $\sigma_8 \Omega_m^{0.25} = 0.599 \pm 0.016$, within 0.4σ of the *Planck* TTTEEE result of Eq. 5b.

¹³ Where θ_{MC} is an approximation to the angular size of the sound horizon at recombination, see Planck Collaboration et al. (2016) for a definition.

BAO point at recombination) to the *Planck* lensing likelihood restricts the range of allowed values of Ω_m resulting in the green contours¹⁴ in Fig. 1. Assuming base Λ CDM, the *Planck* lensing constraints are in very good agreement with the *Planck* TTTEEE results (as they should be, since acoustic peaks of the temperature and polarization power spectra are sensitive to CMB lensing, Larsen et al. see e.g. 2016). Over the redshift range probed by *Planck* lensing, there is no evidence from Fig. 1 for any gravitational slip/modified gravity type of effect that might be causing photons to behave in a different way from the predictions of Λ CDM.

It is possible to test consistency of weak galaxy and CMB lensing at redshifts $z \lesssim 1$ by cross-correlating CMB lensing with weak lensing maps and/or maps of the galaxy distribution (e.g. Marques et al. 2020; Robertson et al. 2021; Krolewski et al. 2021; Chang et al. 2022; Chen et al. 2022a). We will discuss these measurements briefly in Sect. 5.

3 A POSSIBLE SOLUTION

3.1 Motivation

To summarize the previous section:

- (i) There is evidence from independent weak lensing surveys that the amplitude of the matter fluctuations, as measured by the S_8 parameter, is lower than expected according to the *Planck* Λ CDM cosmology at about the $2.5 - 3\sigma$ level.
- (ii) Redshift space distortions analyses over the redshift range $0.02 - 1.6$ are consistent with the *Planck* base Λ CDM cosmology, suggesting that perturbations grow at the rates expected in Λ CDM over this entire redshift range.
- (iii) CMB lensing is consistent with the expectations of the *Planck* base Λ CDM cosmology, suggesting that photons behave as expected in this cosmology and that perturbations grow at the expected rates over the redshift range $z \sim 1000$ to $z \lesssim 2$.
- (iv) In addition, the combination of BAO measurements and magnitude-redshift relation of Type Ia supernovae tightly constrains the expansion history $H(z)$ to be very close to that of the *Planck* base Λ CDM cosmology over the redshift range probed by the weak lensing surveys (Heavens et al. 2014; Verde et al. 2017; Macaulay et al. 2019; Efstathiou 2021). Solutions to the S_8 tension involving a change in the background cosmology (e.g. invoking a late time transition to a phantom equation of state as considered by Joudaki et al. 2017) are disfavoured by the BAO and supernova data.

In this paper we will seek a physical explanation of the S_8 tension that ties together points (i)-(iv).

Figure 3 shows the KiDS ξ_{\pm} measurements as reported in KiDS21. The shaded regions in the ξ_{-} plot shows the range of angular scales that are excluded from the cosmological analysis by KiDS21 to reduce uncertainties associated with the modelling of baryonic feedback. We use the public KiDS pipeline and follow the updated analysis of Tröster et al. (2021), who re-analyse the KiDS21 band-power measurements with HMCODE2020 (Mead et al. 2021) in place

of the earlier version of HMCODE (Mead et al. 2015) used in KiDS21. HMCODE2020 provides a description of the non-linear evolution of the matter power spectrum and models baryonic feedback via a parameter $\Theta_{\text{AGN}} = \log_{10}(T_{\text{AGN}}/\text{K})$ calibrated using the BAHAMAS (BARYons and HALoes of MASSive Systems) hydrodynamical simulations (McCarthy et al. 2017; van Daalen et al. 2020), where T_{AGN} is a sub-grid heating parameter. The solid blue line in this figure shows our best fit to these data applying the same priors on parameters, including Θ_{AGN} , as in (Tröster et al. 2021, see their Appendix A). The marginalised mean value of the S_8 posterior distribution¹⁵ is quoted in Table 1 (entry labelled HMCODE2020 $\Theta_{\text{AGN}} = 7.3 - 8.3$, which we will refer to as the ‘fiducial’ analysis). This is within 0.5σ of the analysis reported in Table 1 using HMCODE2016 (which agrees perfectly with the results of KiDS21), consistent with the impact on the band powers statistics as reported by Tröster et al. (2021, Appendix A). The cosmological parameters for this fit will be discussed further in Sect. 3.3.

The blue dashed lines in Fig. 3 show the predictions for the same parameters but now using only the *linear* theory matter power spectrum. One can see that the non-linear corrections make a dominant contribution to the total signal, even for ξ_{+} except on angular scales $\gtrsim 10 - 20$ arcmin. Evidently, extracting precision cosmology from smaller angular scales requires accurate modelling of the non-linear power spectrum.

Given this sensitivity, we investigate the plausibility of solving the S_8 tension by modifying the spectrum only in the non-linear regime, while fixing the linear power spectrum to that of the *Planck* base Λ CDM cosmology. With such a solution it may possible to explain the cosmic shear measurements in a way that is consistent with points (i)-(iv) above, since the RSD measurements and *Planck* CMB lensing are insensitive to highly non-linear scales. In addition, such a solution would not require any modification to the *Planck* Λ CDM expansion history, preserving the consistency of the Λ CDM model with the magnitude-redshift relation of Type Ia supernovae, and the geometrical constraints from BAO measurements.

3.2 Phenomenological Model

The lensing data are not yet sufficiently precise to allow a parametric reconstruction of the matter power spectrum as a function of redshift, so in this section we adopt a particularly simple phenomenological model. At this stage, we wish to investigate whether a model with the *Planck* Λ CDM cosmological parameters and linear fluctuation spectrum can provide an acceptable fit to the KiDS ξ_{\pm} measurements via a modification of the spectrum in the non-linear regime. We write the matter power spectrum, $P_m(k, z)$, as

$$P_m(k, z) = P_m^{\text{L}}(k, z) + A_{\text{mod}}[P_m^{\text{NL}}(k, z) - P_m^{\text{L}}(k, z)], \quad (6)$$

where the superscript L denotes the linear theory power spectrum, NL denotes the non-linear power spectrum computed by HMCODE2020 with baryonic feedback switched

¹⁴ Computed from the chains ‘base.lenspriors_BAO.theta’ available from the *Planck* Legacy Archive (<https://www.cosmos.esa.int/web/planck/pla>).

¹⁵ Throughout this paper we always report the marginalised mean value of the posterior distribution and the 68% confidence limits.

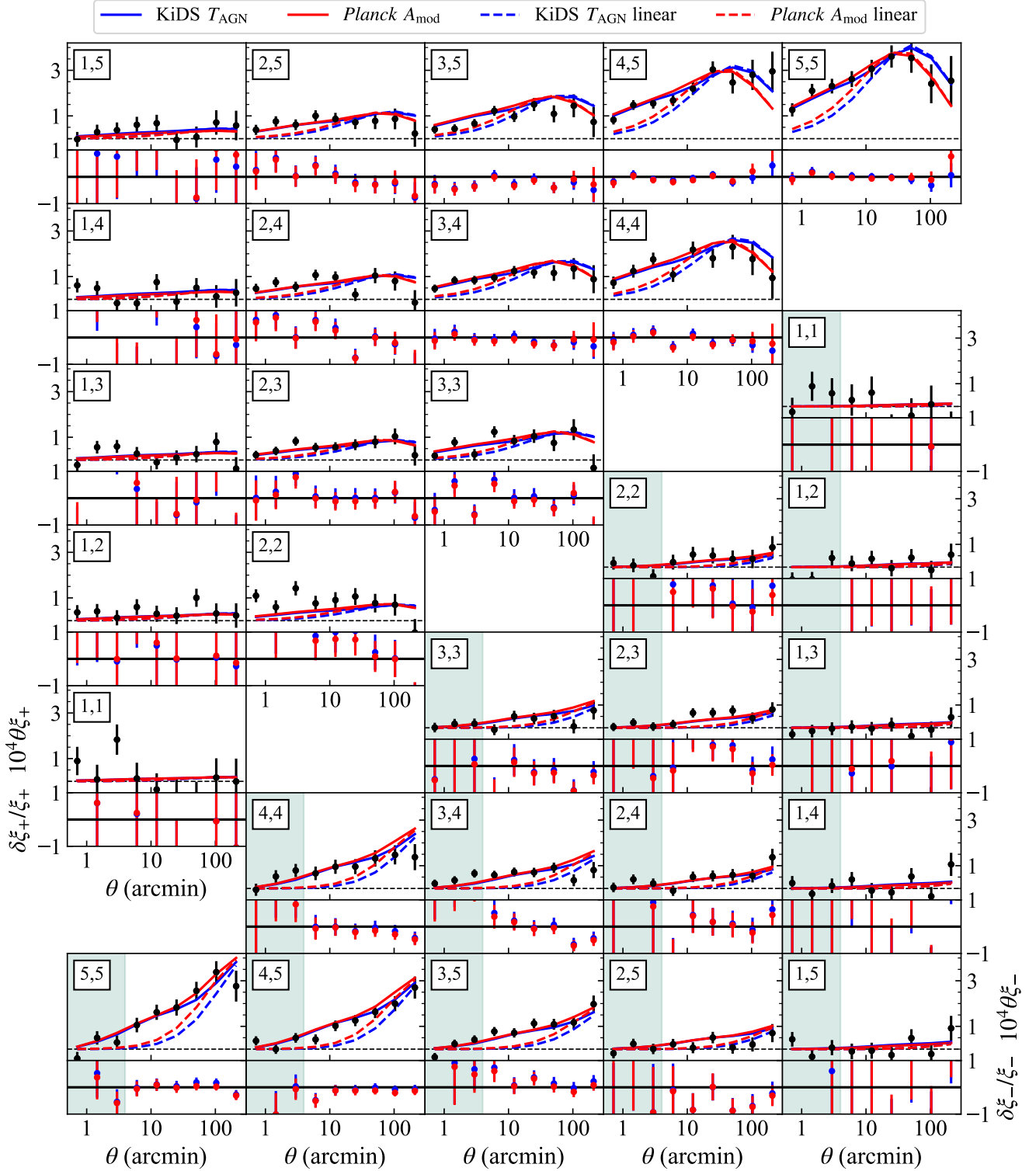


Figure 3. Measurements of KiDS21 two-point correlation functions ξ_{\pm} , scaled by the angular separation, θ (upper panels). The correlation functions are measured for each redshift bin pair, indicated by the label and the error bar represents the square root of the diagonal of the analytic covariance matrix. The blue line is the best fit Λ CDM theoretical prediction, including modelling of the non-linear matter power spectrum using HMCode2020 (very similar to the KiDS21 fit, which used HMCode2016), which includes a baryon feedback parameter Θ_{AGN} . The red line fixes cosmological parameters to the *Planck* best-fit values and now modulates the non-linear power spectrum using the parameter A_{mod} (Eq. 6). In both cases, the dashed lines show ξ_{\pm} computed from the linear matter power spectra. The lower panels show the residual differences between the models and the KiDS21 measurements $\delta\xi_{\pm}/\xi_{\pm}$. Following KiDS21, scales excluded from the analysis are shaded in green.

Table 1. Mean value of S_8 and 1σ errors from our The entry labelled HMCODE2016 uses the identical non-linear matter power spectrum and feedback model as in KiDS21 and reproduces their results to high accuracy. The next set of entries use HMCODE2020 to model the non-linear power spectrum applying uniform priors with different ranges for the baryon feedback parameter Θ_{AGN} . (The row labelled ‘no feedback’ has all baryon feedback switched off.) The asterisk denotes the case of a narrow prior on Θ_{AGN} , as assumed by Tröster et al. (2021), which we refer to as the ‘fiducial’ model in this paper. The final set of entries show results for the phenomenological non-linear suppression model governed by the parameter A_{mod} (see Eq.6). For the cases labelled ‘free’, the cosmological parameters are allowed to vary freely. For cases labelled ‘Planck’ the cosmological parameters are fixed to the TTTEEE values for the *Planck* best fit Λ CDM cosmology. The column labelled N_σ lists $(\chi^2_{\text{min}} - \sqrt{2N_{\text{deg}}})/\sqrt{2N_{\text{deg}}}$ where N_{deg} is the effective number of degrees of freedom. We have $N_{\text{deg}} = 225 - 4.5$ (accounting for the number of constrained parameters in the fits following Joachimi et al. 2021) for the ‘free’ fits where cosmological parameters are allowed to vary in addition to nuisance parameters (see KiDS21) and $N_{\text{deg}} = 225 - 2.5$ for the fits with cosmological parameters constrained to the *Planck* values. The column labelled PTE gives the probability to exceed the value of χ^2_{min} .

Non-linear model & prior range	Cosmology	S_8	χ^2_{min}	N_σ	PTE
HMCODE2016	free	0.765 ± 0.018	260.1	1.92	0.030
HMCODE2020 no feedback	free	0.755 ± 0.016	261.5	1.95	0.025
*HMCODE2020 $\Theta_{\text{AGN}} = 7.3 - 8.3$	free	0.774 ± 0.021	260.2	1.89	0.029
HMCODE2020 $\Theta_{\text{AGN}} = 7.0 - 10.0$	free	0.785 ± 0.030	260.0	1.88	0.030
HMCODE2020 $\Theta_{\text{AGN}} = 7.0 - 10.0$	<i>Planck</i>	0.829	267.6	2.13	0.016
HMCODE2020 $A_{\text{mod}} = 0.5 - 1.2$	free	0.780 ± 0.035	260.3	1.89	0.029
HMCODE2020 $A_{\text{mod}} = 0.5 - 1.2$	<i>Planck</i>	0.829	265.5	2.04	0.021

off and A_{mod} is an amplitude parameter that we vary in the MCMC analysis.

Fixing the cosmology to the *Planck* TTTEEE Λ CDM parameters, but allowing the ‘nuisance’ parameters describing intrinsic alignments, redshift calibration errors and A_{mod} to vary, we find the best fit theory model shown by the solid red line in Fig. 3. As can be seen, this model is almost indistinguishable from the blue line of the KiDS cosmology. The posterior distribution of the parameter A_{mod} is shown in red in Fig. 4. We find a mean

$$A_{\text{mod}} = 0.69 \pm 0.06, \quad (7)$$

and a minimum value of $\chi^2_{\text{min}} = 265.5$ for 225 data points, which is very close to the minimum value of χ^2 for the fiducial model (see Table 1). Both models provide acceptable fits to the data. (All of the χ^2 values listed in Table 1 are high by about 2σ as a consequence of outliers, for example, the points at $\theta \lesssim 50'$ in the (2,2) ξ_+ correlation function). Note that the uncertainty in Eq. 7 is an underestimate as we have neglected the error on the *Planck* base Λ CDM cosmology. The reanalysis of the KiDS-1000 ξ_+ measurements varying both the A_{mod} and cosmological parameters is shown as the blue contour in Fig. 4, highlighting the degeneracy between S_8 and A_{mod} , which reduces the power of lensing data to constrain S_8 .

We find that fixing the cosmology to Planck does not cause any significant shifts to the nuisance parameters compared to the fiducial analysis. Similarly, we have verified that fixing the nuisance parameters to the best fit values of the fiducial analysis constraints does not alter the constraint on A_{mod} . These tests show that the low value of A_{mod} in Eq. 7 is insensitive to the nuisance parameters.

The results of this section show that a suppression of the non-linear power spectrum can reconcile the base *Planck* cosmology with the KiDS lensing data. However, the model is purely phenomenological and so it is reasonable to ask whether such a suppression has a physical interpretation. There are two obvious possibilities: (a) that the suppression is caused by baryonic feedback; (b) that it is caused by a

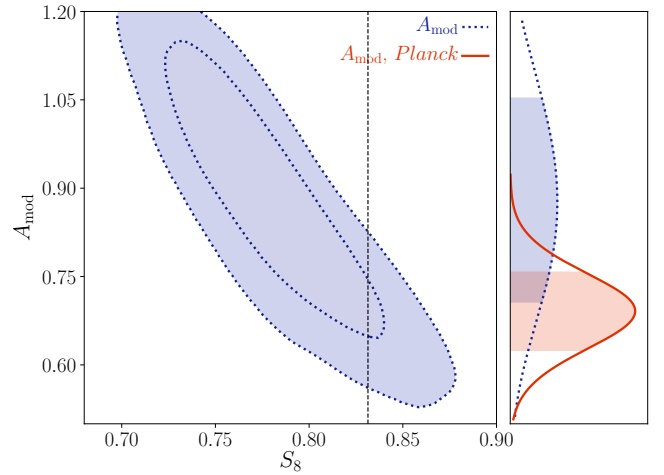


Figure 4. Illustration of the strong degeneracy between S_8 and the phenomenological power spectrum suppression parameter A_{mod} . The blue contours shown in the left-hand panel represent the 68% and 95% constraints for the KiDS ξ_+ statistics analyzed by using HMCODE2020-no feedback, but instead varying A_{mod} . The dashed line indicates the *Planck* Λ CDM best-fit value for the S_8 parameter. The posterior of A_{mod} for this case is shown by the blue curve in the right hand panel. If the cosmological parameters are fixed to the *Planck* Λ CDM best-fit values we find the posterior for A_{mod} shown by the red curve in the right hand panel.

physical property of the dark matter that suppresses the power spectrum on small scales, for example some type of self-interaction (see e.g. the review by Tulin & Yu 2018) or other non-gravitational interaction (e.g. Becker et al. 2021), a mixture of cold and warm dark matter (e.g. Boyarsky et al. 2009), or an axionic dark matter component with a de Broglie wavelength of a few Mpc (e.g. Hui et al. 2017). We consider baryonic feedback in the next subsection.

3.3 Baryonic Feedback

Hydrodynamic simulations of structure formation have improved remarkably over the last decade (e.g. Schaye et al. 2015; McCarthy et al. 2017; Nelson et al. 2019). Nevertheless, the detailed physics involved in baryon cooling, star formation, stellar feedback and feedback from active galactic nuclei (AGN) remains extremely uncertain. As pointed out by many authors, feedback process redistribute the baryons leading to a suppression of the dark matter power spectrum in the non-linear regime (see e.g. van Daalen et al. 2011; Vogelsberger et al. 2014b; Hellwing et al. 2016; Chisari et al. 2019, and references therein). Since feedback processes are not well understood, there is considerable uncertainty in the overall amplitude of this suppression, its scale dependence and evolution with redshift. In this section we use the feedback scheme implemented in HMCODE2020 and ask how far do we have to vary the feedback parameter Θ_{AGN} to match the suppression of our phenomenological model of Eq. 7.

We first pin the cosmological parameters to the *Planck* TTTEEE Λ CDM parameters then fit the KiDS ξ_{\pm} data using HMCODE2020 with a broad prior¹⁶ on Θ_{AGN} that is uniform in the range $7.0 < \Theta_{\text{AGN}} < 10.0$. This prior range is substantially wider than the range $7.6 < \Theta_{\text{AGN}} < 8.0$ over which HMCODE2020 was calibrated against the BAHAMAS simulations. As we move outside the calibrated regime, the link between the parameter Θ_{AGN} and physical models of feedback becomes more tenuous.

The posterior distribution of the Θ_{AGN} parameter is shown in red dashed in Fig. 5 and has a marginalised mean of

$$\Theta_{\text{AGN}} = 9.17^{+0.2}_{-0.8}. \quad (8)$$

As in the previous section, we have verified that fixing the cosmology to *Planck* Λ CDM does not lead to significant differences in the nuisance parameters compared to the fiducial analysis and that fixing the nuisance parameters to their fiducial best-fit values does not change the constraint of Eq. 8. This model gives a minimum value of $\chi^2_{\text{min}} = 267.6$ (see Table 1), almost identical to the minimum value of χ^2 for the A_{mod} model with cosmological parameters fixed to *Planck*. Note that the error in Eq. 8 does not include the uncertainty in the *Planck* base Λ CDM cosmology. As expected, HMCODE2020 with a broad prior on Θ_{AGN} behaves qualitatively like the phenomenological A_{mod} model.

Next, we fit the ξ_{\pm} measurements allowing the cosmological parameters to vary while extending the prior range for Θ_{AGN} in HMCODE2020. We have also performed a fit with baryonic feedback switched off. The parameter constraints for these fits are shown in Fig. 5. Table 1 and gives values for S_8 and χ^2 for these fits. Evidently, the parameters are degenerate and opening up the prior on Θ_{AGN} leads to long tails extending to high values of S_8 . Fig. 5 illustrates clearly how high values of S_8 are disfavoured by the assumed prior on the baryonic feedback model adopted by Tröster et al. (2022).

¹⁶ This test is similar to that of Yoon & Jee (2021), who use HMCODE2016 and KiDS-450.

4 COMPARISON WITH THE EFFECTS OF BARYONIC FEEDBACK IN NUMERICAL SIMULATIONS

Very little is known about the dark matter in the Universe. Therefore, it is possible that a resolution of the S_8 tension along the lines of our A_{mod} parameter is reflective of new physics in the dark sector. However, as the landscape of such new physics is enormous and highly speculative, it is reasonable to investigate first whether the non-linear power suppression required to resolve the S_8 tension can be realized using less exotic physics. The posteriors of the Θ_{AGN} parameter in Fig. 5 show that the KiDS weak lensing data alone are not able to constrain both cosmological parameters and the HMCODE2020 baryonic feedback model. Additional information is therefore necessary to quantify the effects of baryonic feedback on cosmic shear. In this Section we discuss whether the non-linear power spectrum suppression required to reconcile the *Planck* Λ CDM cosmology with KiDS weak lensing is compatible with hydrodynamic numerical simulations that include feedback processes.

The power spectrum suppression required by Eq. 8 is shown by the heavy black lines on the the left-hand side of Fig. 6, together with 1σ error bands. The suppression required by the phenomenological model, Eq. 7, is shown in the right-hand panels. The various coloured lines show the suppression of the matter power spectrum caused by baryonic feedback as predicted by a number of cosmological hydrodynamical simulations at $z = 0$ and $z = 1$. The simulation results are from the library¹⁷ compiled by van Daalen et al. (2020), comprised of the original sources cited in the caption of Fig. 6. For both models, the power spectrum suppression required to reconcile the KiDS cosmic shear measurements with the *Planck* cosmology is more extreme than predicted by most of the hydrodynamic simulations.¹⁸ At $z = 1$, only the C-OWLS simulations with high values of the AGN feedback parameter can match the suppression required in our models, though these models fail to reproduce the local gas fractions in groups and clusters (McCarthy et al. 2017).

Is the power spectrum suppression required to alleviate the S_8 tension too extreme for baryonic feedback? Chisari et al. (2019) provide a comprehensive review of the modelling of baryonic feedback mechanisms in cosmological simulations and their effects on the matter power spectrum. The fiducial BAHAMAS model adopts $\Theta_{\text{AGN}} = 7.8$, since this value reproduces the gas mass fractions in groups and clusters and the galaxy stellar mass function at $z \sim 0.1$ (McCarthy et al. 2017). The prior of $7.3 < \Theta_{\text{AGN}} < 8.3$ used by Tröster et al. (2022) is broader than the range over which

¹⁷ <https://powerlib.strw.leidenuniv.nl>

¹⁸ The DES22 Λ CDM-Optimised analysis shown in Fig. 1 gives a slightly higher value of S_8 compared to the KiDS analysis but is lower than the *Planck* Λ CDM value (as in all previous cosmic shear analyses). DES22 makes different analysis choices compared to KiDS21 e.g. to reduce sensitivity to baryonic feedback (Krause et al. 2021). The DES approach is to apply more conservative angular scale cuts designed to mitigate feedback as predicted by C-OWLS AGN (red dot-dashed line in Fig. 6). A detailed analysis is therefore required to compare and combine the KiDS21 and DES22 results. Nevertheless it is likely that a less extreme non-linear correction is required to explain the DES S_8 tension compared to KiDS.

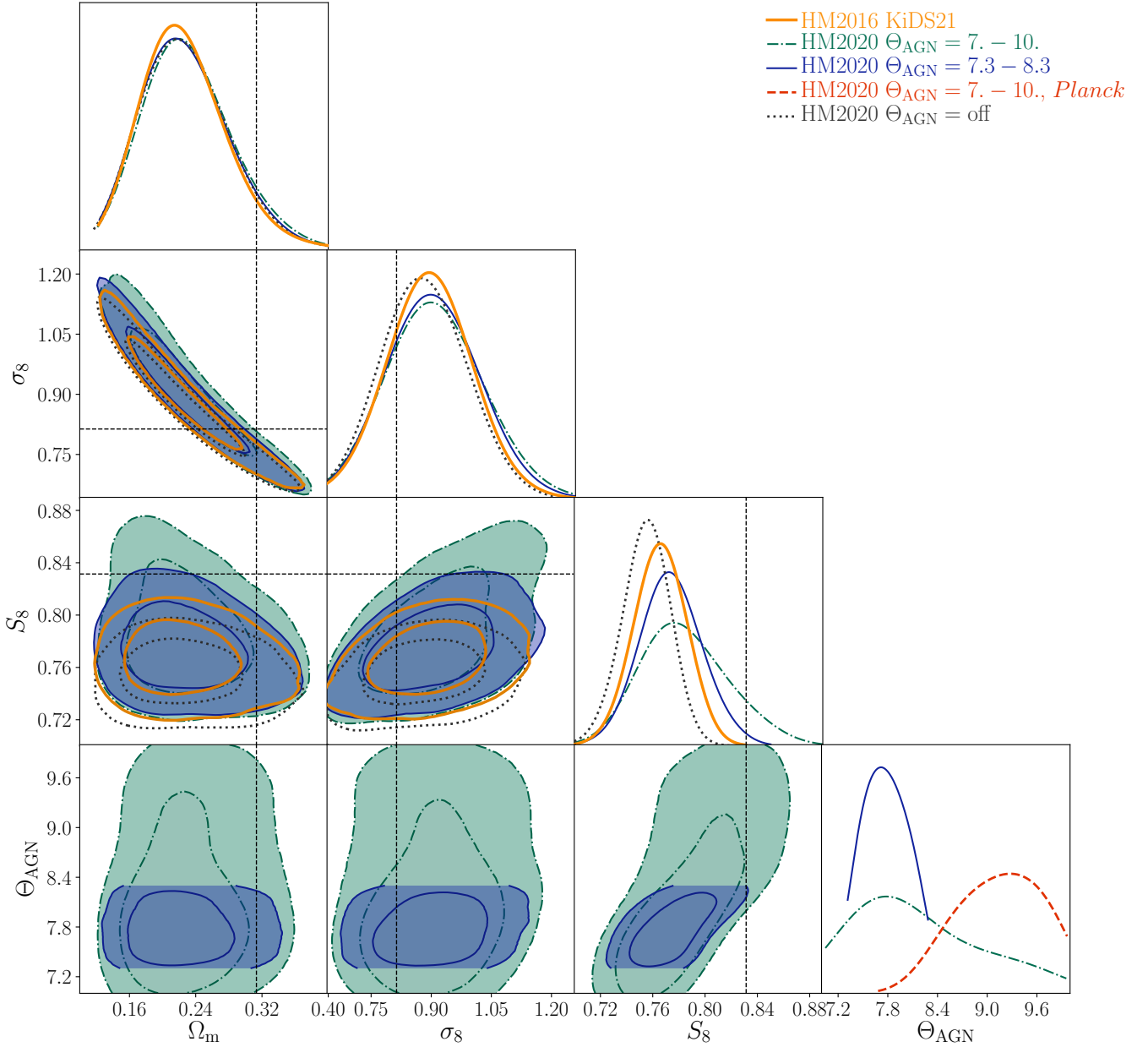


Figure 5. 68% and 95% constraints for KIDS ξ_{\pm} statistics analyzed using HMCODE2020, with varying prior ranges for Θ_{AGN} , compared to the HM2016 analysis by KiDS21 (yellow). Following Tröster et al. (2021), we allow Θ_{AGN} to vary with a uniform prior over the range 7.3 – 8.3 (blue). The range is extended to 7.1 – 10.0 (green) to allow for more extreme feedback. The constraints neglecting feedback are shown in black dotted. We fix the cosmological parameters to *Planck* Λ CDM best fit values and find the posterior on Θ_{AGN} shown by the dashed red line in the bottom right panel. The dashed lines in the other panels show the *Planck* Λ CDM best-fit values for Ω_{m} , σ_8 and S_8 .

HMCODE2020 has been calibrated against the BAHAMAS simulations and is intended to place conservative bounds on physically reasonable models of feedback.

However, as noted by Chisari et al. (2019) baryonic feedback processes are complex and poorly understood. It is perhaps possible that hydrodynamical simulations do not capture the complexities of feedback. For example, it is not feasible to model processes such as black hole growth, magnetic fields, jet formation, cosmic ray injection ab initio. (see e.g. Enßlin et al. 2011; Hopkins et al. 2021; Beckmann et al.

2022). It is also not clear whether simulations calibrated on the local gas fractions of groups and clusters can be extrapolated to redshifts $z \sim 0.5 - 1$ relevant to the interpretation of cosmic shear surveys. It is therefore important to develop empirical ways of constraining baryon feedback rather than relying on numerical simulations.

Joint analyses and cross-correlations between cosmic shear and the kinetic and thermal Sunyaev-Zeldovich (SZ) effects (e.g. Schneider et al. 2021; Tröster et al. 2022) offer a promising way of testing baryonic feedback. In particu-

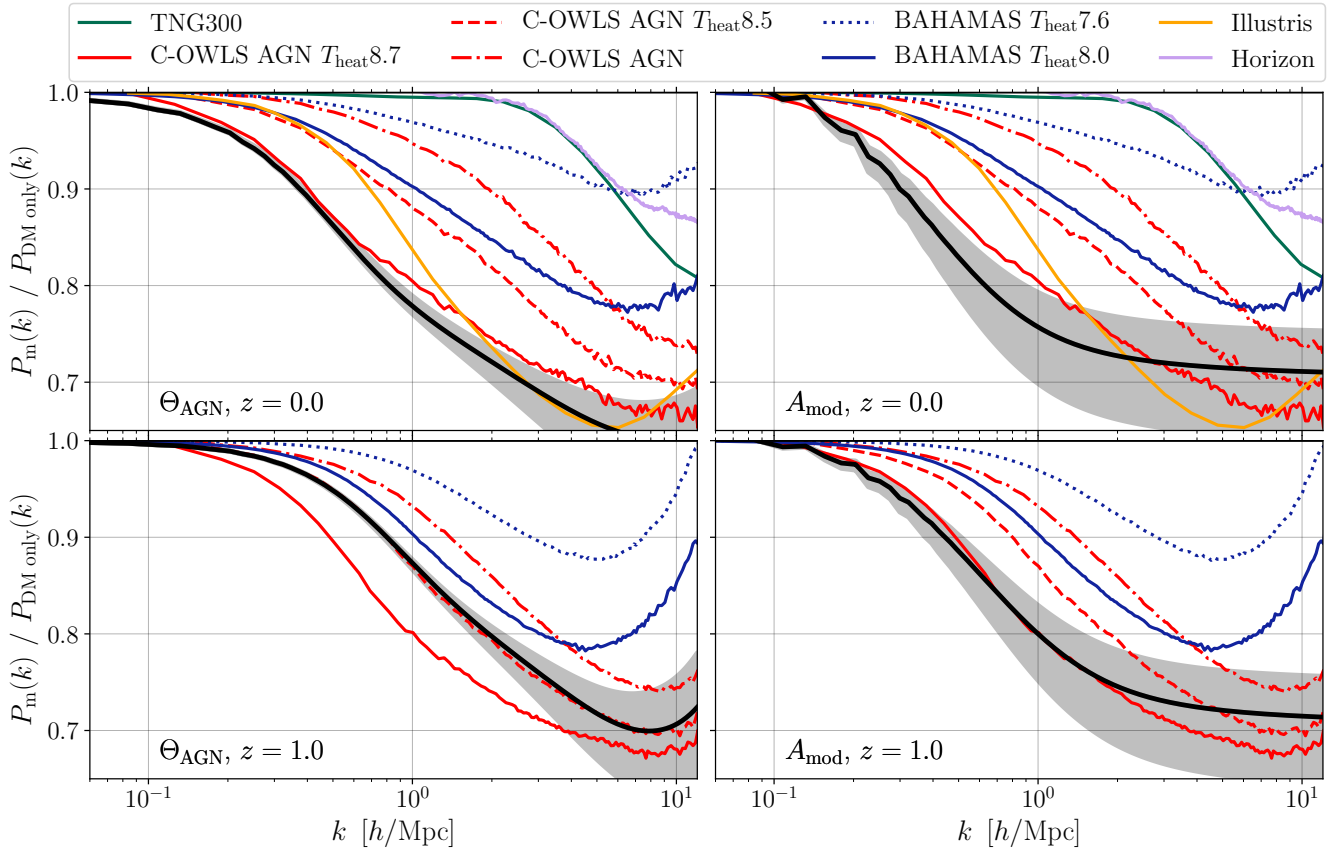


Figure 6. The suppression of the matter power spectrum, $P_m(k)/P_{\text{DM only}}(k)$, required to match the KiDS ξ_{\pm} measurements assuming the *Planck* Λ CDM cosmology. The upper and lower panels show the suppression at $z = 0$ and $z = 1$ respectively. The left hand panels show the HMCode2020 model of Eq. 8 and the right hand panel shows the phenomenological model of Eq. 7. The grey bands show the 1σ allowed ranges. The coloured lines, taken from van Daalen et al. (2020), show the suppression measured from cosmological hydrodynamical simulations incorporating baryonic feedback. The sources are as follows: Illustris (yellow; Vogelsberger et al. 2014a), Illustris TNG300 (green; Springel et al. 2018), Horizon (purple; Dubois et al. 2014), C-OWLS (red; COSMO-Overwhelmingly Large Simulations Le Brun et al. 2014) and BAHAMAS (blue; McCarthy et al. 2017) for several values of their AGN subgrid heating parameters, $\log_{10}(\Delta T_{\text{heat}}/\text{K})$.

lar, SZ observations are sensitive to baryons on larger spatial scales than X-ray observations. Schneider et al. (2021) use the shear power spectrum measurements from KiDS21, Atacama Cosmology Telescope (ACT) measurements of the kinetic SZ (Schaan et al. 2021), together with gas and stellar fractions in groups and clusters inferred from X-ray measurements (Giri & Schneider 2021) to reconstruct the non-linear suppression of power using their baryonification model of feedback. If they constrain the baryon fraction to be within the range allowed by the CMB, they find a power suppression (their Fig. 7) that is extreme than most of the simulations, including BAHAMAS. In particular, they find evidence for a significant suppression of power at the wavenumbers $\lesssim 1 h\text{Mpc}^{-1}$ in good agreement with our best fit A_{mod} model. The cross-correlation analysis of Tröster et al. (2022) of the *Planck* thermal SZ and shear power spectrum measurements supports high values of Θ_{AGN} that are more extreme than predictions from BAHAMAS, but are restricted by the prior range adopted for Θ_{AGN} (a similar effect can be seen in Fig. 5). Hints for more extreme feedback have also been found from other analyses that utilise ACT SZ information Amodeo et al. (2021); Pandey et al. (2021).

To summarize, our analysis shows that a suppression of power extending to large scales corresponding to wavenumbers of $k \sim 0.2 h\text{Mpc}^{-1}$ is required if the *Planck* Λ CDM cosmology is to be reconciled with cosmic shear. Such strong feedback on large scales is not seen in most of the hydrodynamical simulations shown in Fig. 6. If such extreme baryonic feedback can be ruled out, then a non-linear solution to the S_8 tension would probably require new dark matter physics.

5 CONCLUSIONS

This paper is motivated by the substantial evidence from galaxy lensing measurements that the parameter S_8 has a lower value than expected in the *Planck* Λ CDM cosmology. Noting that the signal-to-noise driving the cosmic shear constraints is dominated by non-linear scales, we have investigated whether the *Planck* Λ CDM cosmology can be reconciled with these measurements by modifying the matter power spectrum on non-linear scales, preserving all other features of Λ CDM. If this explanation is correct:

- growth rate measurements that are sensitive mainly to

linear scales, in particular, precision measurements of RSD from wavenumbers $k \lesssim 0.1 h\text{Mpc}^{-1}$ using forthcoming data from the Dark Energy Spectroscopic Instrument (DESI; DESI Collaboration et al. 2016), should agree with the *Planck* cosmology.

- the background expansion history, $H(z)$, and consequently luminosity and angular diameter distances, should agree with the *Planck* ΛCDM cosmology at all redshifts;
- photons should respond to gravity as expected in General Relativity. Gravitational lensing measurements (based on either the CMB or galaxies) that are sensitive primarily to linear scales, should agree with the *Planck* ΛCDM cosmology at all redshifts;

A detailed analysis of the two-point correlation functions ξ_{\pm} , as measured by KiDS21, shows that the *Planck* ΛCDM model can provide acceptable fits if the power-spectrum on non-linear scales is suppressed via our phenomenological model of Eq. 4, with a value $A_{\text{mod}} \approx 0.69$. If this suppression is interpreted as being caused by baryonic feedback, then a comparison with numerical hydrodynamic simulations shows that strong baryonic feedback is required. The amplitude and spatial extent of the suppression that we require are well outside the ranges found in the BAHAMAS simulations and cannot be reproduced by baryonic feedback models adopted in KiDS21 and Tröster et al. (2021) given their choices of priors. However, the physics of baryonic feedback is extremely complex and multi-scale and it may be premature to exclude models with strong baryonic feedback. As mentioned in Sect. 3.3, combinations of cosmic shear with thermal and kinetic SZ measurements provide hints that baryonic feedback may be stronger than conventionally thought (Amodeo et al. 2021; Schneider et al. 2021; Tröster et al. 2022). In particular, kinetic SZ measurements offer the possibility of constraining the effects of baryonic feedback into the mildly non-linear regime.

Recently some evidence for low values of S_8 , though not at high statistical significance, has come from cross-correlations of CMB lensing with photometric galaxy catalogues (Marques et al. 2020; Robertson et al. 2021; Hang et al. 2021; Krolewski et al. 2021; Chang et al. 2022; White et al. 2022), or with galaxy redshift surveys (Chen et al. 2022a). In some of these analyses, modifications to the non-linear power spectrum as proposed in this paper may increase the inferred values of S_8 . For others (e.g. Chen et al. 2022a) the low values of S_8 are driven by cross-correlations at large angular scales that are insensitive to the non-linear power spectrum but may be affected by selection biases. An analysis of galaxy-lensing cross-correlations shows that the preference for low values of S_8 comes from measurements at small scales (Amon et al. 2022a).

It is important to recognise the possibility that a suppression of the matter power spectrum on non-linear scales may be a consequence of new physics in the dark sector. For example, a suppression would arise if a fraction of the dark matter were in the form of a light axionic particle with a de Broglie wavelength of a few Mpc (Widrow & Kaiser 1993; Hu et al. 2000; Hui et al. 2017) though there are many other possibilities as discussed by Hooper et al. (2022). More detailed investigations of such models would be worthwhile, particularly if it can be demonstrated definitively that baryonic feedback cannot solve the S_8 tension. In the longer term, it

may be possible to differentiate between baryonic feedback and the physics of dark matter by measuring the redshift dependence of the matter power spectrum suppression (Viel et al. 2013) and using the high redshift reach of the quasar Lyman- α forest as discussed by Hooper et al. (2022).

ACKNOWLEDGEMENTS

We are particularly grateful to Catherine Heymans and Hendrik Hildebrandt for a careful reading of a draft of this paper. We thank Florian Buetler, Oliver Philcox, Licia Verde and Zvonimir Vlah for correspondence on redshift space distortions and Guido D’Amico, Leonardo Senatore and collaborators, for sharing their MCMC chains that we used in Fig. 1. We indebted to Joe Zuntz for developing and maintaining the COSMOSIS framework (Zuntz et al. 2015).

AA receives support from a Kavli Fellowship at Cambridge University. Based on observations made with ESO Telescopes at the La Silla Paranal Observatory under programme IDs 177.A-3016, 177.A-3017, 177.A-3018 and 179.A-2004, and on data products produced by the KiDS consortium. The KiDS production team acknowledges support from: Deutsche Forschungsgemeinschaft, ERC, NOVA and NWO-M grants; Target; the University of Padova, and the University Federico II (Naples).

REFERENCES

- Abdalla E., et al., 2022, *Journal of High Energy Astrophysics*, **34**, 49
- Aiola S., et al., 2020, *J. Cosmology Astropart. Phys.*, **2020**, 047
- Alam S., et al., 2017, *MNRAS*, **470**, 2617
- Alam S., et al., 2021, *Phys. Rev. D*, **103**, 083533
- Amodeo S., et al., 2021, *Phys. Rev. D*, **103**, 063514
- Amon A., et al., 2022a, arXiv e-prints, p. arXiv:2202.07440
- Amon A., et al., 2022b, *Phys. Rev. D*, **105**, 023514
- Asgari M., et al., 2020, *A&A*, **634**, A127
- Asgari M., et al., 2021, *A&A*, **645**, A104
- Becker N., Hooper D. C., Kahlhoefer F., Lesgourgues J., Schöneberg N., 2021, *J. Cosmology Astropart. Phys.*, **2021**, 019
- Beckmann R. S., Dubois Y., Pellisier A., Olivares V., Polles F. L., Hahn O., Guillard P., Lehnert M. D., 2022, arXiv e-prints, p. arXiv:2204.03629
- Benisty D., 2021, *Physics of the Dark Universe*, **31**, 100766
- Bennett C. L., et al., 2013, *ApJS*, **208**, 20
- Bertschinger E., 2011, *Philosophical Transactions of the Royal Society of London Series A*, **369**, 4947
- Betoule M., et al., 2014, *A&A*, **568**, A22
- Beutler F., et al., 2011, *MNRAS*, **416**, 3017
- Blomqvist M., et al., 2019, *A&A*, **629**, A86
- Boruah S. S., Hudson M. J., Lavaux G., 2020, *MNRAS*, **498**, 2703
- Boyardsky A., Lesgourgues J., Ruchayskiy O., Viel M., 2009, *J. Cosmology Astropart. Phys.*, **2009**, 012
- Brieden S., Gil-Marín H., Verde L., 2021a, *Phys. Rev. D*, **104**, L121301
- Brieden S., Gil-Marín H., Verde L., 2021b, *J. Cosmology Astropart. Phys.*, **2021**, 054
- Brieden S., Gil-Marín H., Verde L., 2022, arXiv e-prints, p. arXiv:2204.11868
- Brout D., et al., 2021, arXiv e-prints, p. arXiv:2112.03864
- Carron J., Mirmelstein M., Lewis A., 2022, arXiv e-prints, p. arXiv:2206.07773
- Chang C., et al., 2022, arXiv e-prints, p. arXiv:2203.12440

- Chen S.-F., White M., DeRose J., Kokron N., 2022a, arXiv e-prints, p. [arXiv:2204.10392](#)
- Chen S.-F., Vlah Z., White M., 2022b, *J. Cosmology Astropart. Phys.*, 2022, 008
- Chisari N. E., et al., 2019, *The Open Journal of Astrophysics*, 2, 4
- Cooke R. J., Pettini M., Steidel C. C., 2018, *ApJ*, 855, 102
- D’Amico G., Donath Y., Lewandowski M., Senatore L., Zhang P., 2022, arXiv e-prints, p. [arXiv:2206.08327](#)
- DES Collaboration et al., 2021, arXiv e-prints, p. [arXiv:2105.13549](#)
- DESI Collaboration et al., 2016, arXiv e-prints, p. [arXiv:1611.00036](#)
- Daniel S. F., Caldwell R. R., Cooray A., Melchiorri A., 2008, *Phys. Rev. D*, 77, 103513
- Dubois Y., et al., 2014, *MNRAS*, 444, 1453
- Dutcher D., et al., 2021, *Phys. Rev. D*, 104, 022003
- Efstathiou G., 2021, *MNRAS*, 505, 3866
- Efstathiou G., Gratton S., 2021, *The Open Journal of Astrophysics*, 4, 8
- Efstathiou G., Lemos P., 2018, *MNRAS*, 476, 151
- Enßlin T., Pfrommer C., Miniati F., Subramanian K., 2011, *A&A*, 527, A99
- Freedman W. L., 2021, arXiv e-prints, p. [arXiv:2106.15656](#)
- Freedman W. L., et al., 2019, *ApJ*, 882, 34
- Freedman W. L., et al., 2020, *ApJ*, 891, 57
- García-García C., Ruiz Zapatero J., Alonso D., Bellini E., Ferreira P. G., Mueller E.-M., Nicola A., Ruiz-Lapuente P., 2021, arXiv e-prints,
- Giri S. K., Schneider A., 2021, *J. Cosmology Astropart. Phys.*, 2021, 046
- Hamana T., et al., 2020, *PASJ*, 72, 16
- Hang Q., Alam S., Peacock J. A., Cai Y.-C., 2021, *MNRAS*, 501, 1481
- Heavens A., Jimenez R., Verde L., 2014, *Phys. Rev. Lett.*, 113, 241302
- Hellwing W. A., Schaller M., Frenk C. S., Theuns T., Schaye J., Bower R. G., Crain R. A., 2016, *MNRAS*, 461, L11
- Heymans C., et al., 2013, *MNRAS*, 432, 2433
- Heymans C., et al., 2021, *A&A*, 646, A140
- Hikage C., et al., 2019, *PASJ*, 71, 43
- Hildebrandt H., et al., 2021, *A&A*, 647, A124
- Hooper D. C., Schöneberg N., Murgia R., Archidiacono M., Lesgourgues J., Viel M., 2022, arXiv e-prints, p. [arXiv:2206.08188](#)
- Hopkins P. F., Chan T. K., Ji S., Hummels C. B., Kereš D., Quataert E., Faucher-Giguère C.-A., 2021, *MNRAS*, 501, 3640
- Howlett C., Ross A. J., Samushia L., Percival W. J., Manera M., 2015, *MNRAS*, 449, 848
- Hu W., Barkana R., Gruzinov A., 2000, *Phys. Rev. Lett.*, 85, 1158
- Hui L., Ostriker J. P., Tremaine S., Witten E., 2017, *Phys. Rev. D*, 95, 043541
- Huterer D., Shafer D. L., Scolnic D. M., Schmidt F., 2017, *J. Cosmology Astropart. Phys.*, 5, 015
- Ivanov M. M., 2021, *Phys. Rev. D*, 104, 103514
- Ivanov M. M., Simonović M., Zaldarriaga M., 2020, *J. Cosmology Astropart. Phys.*, 2020, 042
- Joachimi B., et al., 2021, *A&A*, 646, A129
- Joudaki S., et al., 2017, *MNRAS*, 471, 1259
- Kaiser N., 1987, *MNRAS*, 227, 1
- Kannawadi A., et al., 2019, *A&A*, 624, A92
- Kazantzidis L., Perivolaropoulos L., 2018, *Phys. Rev. D*, 97, 103503
- Krause E., et al., 2021, arXiv e-prints, p. [arXiv:2105.13548](#)
- Krolewski A., Ferraro S., White M., 2021, *J. Cosmology Astropart. Phys.*, 2021, 028
- Lahav O., Lilje P. B., Primack J. R., Rees M. J., 1991, *MNRAS*, 251, 128
- Larsen P., Challinor A., Sherwin B. D., Mak D., 2016, *Phys. Rev. Lett.*, 117, 151102
- Le Brun A. M. C., McCarthy I. G., Schaye J., Ponman T. J., 2014, *MNRAS*, 441, 1270
- MacCrann N., et al., 2022, *MNRAS*, 509, 3371
- Macaulay E., Wehus I. K., Eriksen H. K., 2013, *Phys. Rev. Lett.*, 111, 161301
- Macaulay E., et al., 2019, *MNRAS*, 486, 2184
- Mandelbaum R., et al., 2018, *MNRAS*, 481, 3170
- Marques G. A., Liu J., Huffenberger K. M., Colin Hill J., 2020, *ApJ*, 904, 182
- McCarthy I. G., Schaye J., Bird S., Le Brun A. M. C., 2017, *MNRAS*, 465, 2936
- Mead A. J., Peacock J. A., Heymans C., Joudaki S., Heavens A. F., 2015, *MNRAS*, 454, 1958
- Mead A. J., Brieden S., Tröster T., Heymans C., 2021, *MNRAS*, 502, 1401
- Myles J., et al., 2021, *MNRAS*, 505, 4249
- Nelson D., et al., 2019, *Computational Astrophysics and Cosmology*, 6, 2
- Nesseris S., Pantazis G., Perivolaropoulos L., 2017, *Phys. Rev. D*, 96, 023542
- Nunes R. C., Vagnozzi S., 2021, *MNRAS*, 505, 5427
- Pandey S., et al., 2021, arXiv e-prints, p. [arXiv:2108.01601](#)
- Philcox O. H. E., Ivanov M. M., 2021, arXiv e-prints, p. [arXiv:2112.04515](#)
- Pizzuti L., Saltas I. D., Casas S., Amendola L., Biviano A., 2019, *MNRAS*, 486, 596
- Planck Collaboration et al., 2016, *A&A*, 594, A13
- Planck Collaboration et al., 2020a, *A&A*, 641, A6
- Planck Collaboration et al., 2020b, *A&A*, 641, A8
- Riess A. G., et al., 2016, *The Astrophysical Journal*, 826, 56
- Riess A. G., Casertano S., Yuan W., Macri L. M., Scolnic D., 2019, *The Astrophysical Journal*, 876, 85
- Riess A. G., Casertano S., Yuan W., Bowers J. B., Macri L., Zinn J. C., Scolnic D., 2021, *ApJ*, 908, L6
- Robertson N. C., et al., 2021, *A&A*, 649, A146
- Ross A. J., Samushia L., Howlett C., Percival W. J., Burden A., Manera M., 2015, *MNRAS*, 449, 835
- Schaan E., et al., 2021, *Phys. Rev. D*, 103, 063513
- Schaye J., et al., 2015, *MNRAS*, 446, 521
- Schneider P., Eifler T., Krause E., 2010, *A&A*, 520, A116
- Schneider A., Giri S. K., Amodeo S., Refregier A., 2021, arXiv e-prints, p. [arXiv:2110.02228](#)
- Scolnic D. M., et al., 2017, preprint, ([arXiv:1710.00845](#))
- Secco L. F., et al., 2022, *Phys. Rev. D*, 105, 023515
- Shah P., Lemos P., Lahav O., 2021, arXiv e-prints, p. [arXiv:2109.01161](#)
- Simpson F., et al., 2013, *MNRAS*, 429, 2249
- Springel V., et al., 2018, *MNRAS*, 475, 676
- Tröster T., et al., 2020, *A&A*, 633, L10
- Tröster T., et al., 2021, *A&A*, 649, A88
- Tröster T., et al., 2022, *A&A*, 660, A27
- Tulin S., Yu H.-B., 2018, *Phys. Rep.*, 730, 1
- Verde L., Bernal J. L., Heavens A. F., Jimenez R., 2017, *MNRAS*, 467, 731
- Viel M., Schaye J., Booth C. M., 2013, *MNRAS*, 429, 1734
- Vogelsberger M., et al., 2014a, *MNRAS*, 444, 1518
- Vogelsberger M., et al., 2014b, *Nature*, 509, 177
- White M., et al., 2022, Cosmological constraints from the tomographic cross-correlation of DESI Luminous Red Galaxies and Planck CMB lensing ([arXiv:2111.09898](#)), [doi:10.1088/1475-7516/2022/02/007](#)
- Widrow L. M., Kaiser N., 1993, *ApJ*, 416, L71
- Wong K. C., et al., 2020, *MNRAS*, 498, 1420
- Yoon M., Jee M. J., 2021, *ApJ*, 908, 13
- Zuntz J., et al., 2015, *Astronomy and Computing*, 12, 45

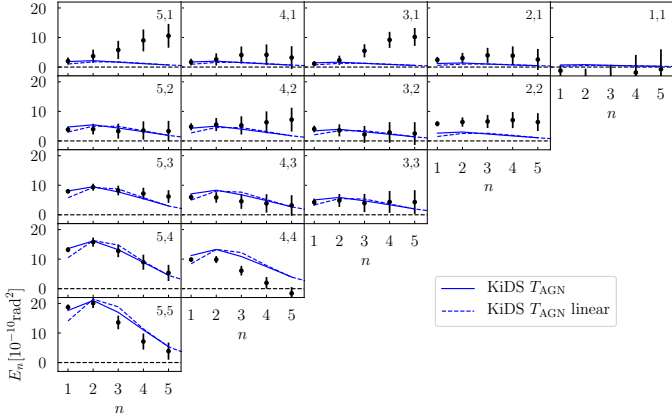


Figure A1. Measurements of KiDS21 COSEBI coefficients, E_n , together with 1σ error bars. The numbers in each panel denote the photometric redshift bins used in each cross-correlation as in Fig. 3 and a zero line is shown for reference (black dotted). The blue line is the best fit Λ CDM theoretical prediction, including modelling of the non-linear matter power spectrum using HMCode2020 (very similar to the KiDS21 fit, which used HMCode2016), which includes a baryon feedback parameter Θ_{AGN} as in our fiducial analysis. The dashed lines indicate the predictions based upon only the *linear* matter power spectra.

d’Amico G., Gleyzes J., Kokron N., Markovic K., Senatore L., Zhang P., Beutler F., Gil-Marín H., 2020, *J. Cosmology Astropart. Phys.*, 2020, 005
 de Sainte Agathe V., et al., 2019, *A&A*, 629, A85
 van Daalen M. P., Schaye J., Booth C. M., Dalla Vecchia C., 2011, *MNRAS*, 415, 3649
 van Daalen M. P., McCarthy I. G., Schaye J., 2020, *MNRAS*, 491, 2424

APPENDIX A: COSEBIS

The fiducial analysis in KiDS21 is based on the COSEBI statistic E_n . The COSEBI statistics are constructed from linear combinations of ξ_{\pm} to separate the signals from E - and B -mode lensing:

$$E_n = \frac{1}{2} \int_{\theta_{\min}}^{\theta_{\max}} [T_{+n}(\theta)\xi_+(\theta) + T_{-n}(\theta)\xi_-(\theta)], \quad (\text{A1a})$$

$$B_n = \frac{1}{2} \int_{\theta_{\min}}^{\theta_{\max}} [T_{+n}(\theta)\xi_+(\theta) - T_{-n}(\theta)\xi_-(\theta)], \quad (\text{A1b})$$

where n is an integer and the filter functions T_n depend on the choices of θ_{\min} and θ_{\max} . Weak lensing should generate pure E modes and so the detection of a B -mode signal is a signature of systematics in the cosmic shear catalogues.

For KiDS-1000, the B -mode signal is consistent with zero. KiDS21 chose to analyze the first five n -modes of E_n , as plotted in Fig. A1. The weighting of wavenumbers in the statistic E_n depends on the range of θ_{\min} and θ_{\max} . For the choices in KiDS21, $0.5' \leq \theta \leq 300'$, the E_n statistic gives lower weight to high wavenumbers in comparison to their ξ_{\pm} data vector and is therefore less sensitive to their baryonic feedback model and other small-scale systematics (Asgari et al. 2020).

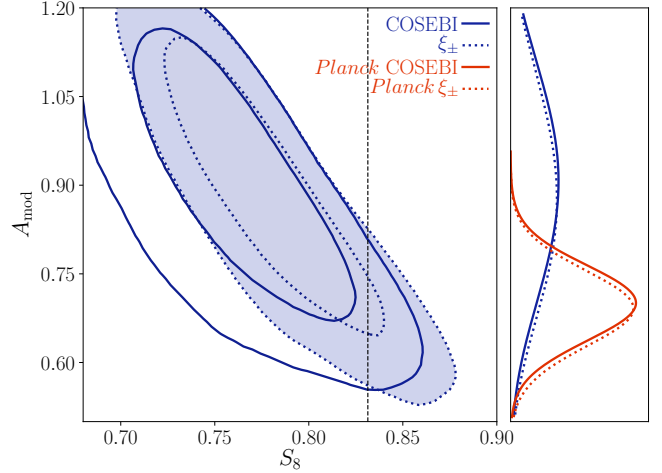


Figure A2. Version of Fig. 4 illustrating the strong degeneracy between S_8 and the phenomenological power spectrum suppression parameter A_{mod} but including results from the COSEBIS statistics. The left hand panel shows the constraints from on A_{mod} and S_8 allowing cosmological and nuisance parameters to vary but with baryonic feedback set to zero. The solid blue contours show the constraints using the COSEBIS, while the dotted blue contours show the results based on ξ_{\pm} (which are the same as those plotted in Fig. 4). The dashed line indicates the *Planck* Λ CDM best-fit value for the S_8 parameter. The posteriors of A_{mod} are shown by the blue and dashed curves in the right hand panel. If the cosmological parameters are fixed to the *Planck* Λ CDM best-fit values we find the posterior for A_{mod} shown by the red curves in the right hand panel.

However, the E_n statistic does retain sensitivity to non-linear scales and to baryonic physics, as is illustrated in Fig. A2 and Fig. A1. The solid line in Fig. A1 shows the best fit to E_n using HMCode2020) with our fiducial prior on Θ_{AGN} . The dashed line shows the prediction based upon the linear power spectrum for this fit. One can see that the sensitivity to non-linearities (and therefore to baryonic feedback), for their choices of θ_{\min} and θ_{\max} , is restricted almost exclusively to the E_1 coefficients which carry much higher statistical weight in the likelihood than the coefficients with $n > 1$. As a consequence, the E_n statistic has very little shape discrimination. Figure A2 illustrates that the COSEBIS and ξ_{\pm} show a similarly strong degeneracy between A_{mod} and S_8 , though the COSEBI contours are considerably wider than those for ξ_{\pm} .

Another consequence of using COSEBIS is that they introduce a correlation between S_8 and Ω_m that extends to low values of S_8 at high values of Ω_m that are strongly disfavoured by *Planck*. As discussed by KiDS21, the COSEBIS constraints on the parameter combination $\Sigma_8 = \sigma_8(\Omega_m/0.3)^{0.54}$ are almost independent of Ω_m . In assessing consistency with *Planck* Λ CDM it is better to use the posterior distribution of Σ_8 rather than S_8 . Similar remarks apply to the Tröster et al. (2022) analysis, which is based on the lensing power spectrum band powers.